Studies of turbulent boundary layer flow through direct numerical simulation

by

Martin Skote

Typsatt i $\mathcal{A}_{\mathcal{M}}\mathcal{S}$-LaTeX.

Studies of turbulent boundary layer flow through direct numerical simulation

Martin Skote

Department of Mechanics, Royal Institute of Technology

SE-100 44 Stockholm, Sweden

Abstract

The objective has been to study turbulent boundary layers under adverse pressure gradients (APG) through direct numerical simulation (DNS). The numerical code is based on a pseudo-spectral technique which is suitable for the simple geometry (flat plate) considered here. A large effort has been put into the optimization of the numerical code on various super computers. Five large simulations have been performed, ranging from a zero pressure gradient boundary layer to a separating flow. The simulations have revealed many features of APG turbulent boundary layers which are difficult to capture in experiments. Especially the near-wall behavior has been investigated thoroughly, both through the statistical and instantaneous flow.

Theoretical work based on the turbulent boundary layer equation has been conducted with the aim to develop near-wall laws suitable for turbulence models. The conditions for self-similarity and relations between mean flow parameters have been reviewed and applied in the DNS. The results from the simulations have confirmed the theoretical part of this work.

The turbulent flows have also been investigated using turbulence models. A boundary layer under strong APG is difficult to predict correctly, and the separating boundary layer is one of the most difficult flows in this respect. The near-wall damping was improved by comparing DNS data and model predictions. The asymptotic behavior of an APG boundary layer for large Reynolds numbers has been determined through asymptotic analysis and with the aid of turbulence models.

The DNS data have also been utilized for the investigation of instantaneous turbulence structures. The turbulent boundary layer was found to be populated by near-wall low-speed streaks and vortices shaped like a horseshoe, in agreement with earlier investigations. The instability mechanism behind the formation of these vortices is examined through a simulation of an artificial low-speed streak introduced in a laminar boundary layer.

The turbulence statistics from the simulations have also been compared with other simulations of turbulent boundary layers and Couette flow.

Descriptors: Turbulence, direct numerical simulation, boundary layer, separation, parallel computers, turbulence modelling.

Preface

This thesis considers direct numerical simulation of turbulent boundary layer flows. The introductory part is a summary of the work contained in the nine papers included, and thus is not a general review of the subject. The thesis is based on and contains the following papers.

Paper 1. SKOTE, M., HENNINGSON, D.S. & HENKES, R.A.W.M. 1998 Direct numerical simulation of self-similar turbulent boundary layers in adverse pressure gradients. *Flow, Turbulence and Combustion*, **60**, 47–85.

Paper 2. HENKES, R.A.W.M., SKOTE, M. & HENNINGSON, D.S. 1997 Application of turbulence models to equilibrium boundary layers under adverse pressure gradient. *Eleventh Symposium on Turbulent Shear Flows, Grenoble, France*, 33:13–33:18.

Paper 3. SKOTE, M. & HENNINGSON, D.S. 1999 Analysis of the data base from a DNS of a separating turbulent boundary layer. *Center for Turbulence Research, Annual Research Briefs 1999*, 225–237.

Paper 4. SKOTE, M. & HENNINGSON, D.S. 2000 Direct numerical simulation of separating turbulent boundary layers. Submitted to *Journal of Fluid Mechanics.*

Paper 5. SKOTE, M. & WALLIN, S. 2000 Near-wall damping in model predictions of separated flows. FFA TN 2000-72.

Paper 6. KOMMINAHO, J. & SKOTE, M. 2000 Reynolds stress budgets in Couette and boundary layer flows. Submitted to *Flow, Turbulence and Combustion.*

Paper 7. SKOTE, M., HARITONIDIS J.H. & HENNINGSON, D.S. 2000 Instabilities in turbulent boundary layers. Submitted to *Physics of Fluids.*

Paper 8. ALVELIUS, K. & SKOTE, M. 1999 The performance of a spectral simulation code for turbulence on parallel computers with distributed memory. TRITA-MEK 2000:17.

Paper 9. LUNDBLADH, A., BERLIN, S., SKOTE, M., HILDINGS, C., CHOI, J., KIM, J. & HENNINGSON, D.S. 1999 An efficient spectral method for simulation of incompressible flow over a flat plate. TRITA-MEK 1999:11.

The papers are re-set in the present thesis format. Some of them are based on publications in conference proceedings (Skote & Henningson 1997, 1998, 1999; Skote *et al.* 2000).

Division of work between authors

The DNS was performed with a numerical code already in use for mainly transition research. It is based on a pseudo-spectral technique and has been further developed by Skote (MS) for extracting flow quantities needed in turbulence research. The necessary changes of the code for the porting to computers with distributed memory have been completed.

The DNS in paper 1 was performed by MS. The turbulence model calculations were done by MS together with Henkes (RH). The theoretical work was performed by MS. The writing was done by MS with great help from Henningson (DH).

The DNS data in paper 2 are the same as in paper 1. The model predictions were conducted by RH. The paper was written mainly by RH.

The DNS data in paper 3 were taken from Na & Moin (1998). The evaluation of the data and the writing was done by MS with help from DH. The theoretical part of the work was done by MS.

The DNS in paper 4 was performed by MS. The theoretical work was done by MS. The writing was done by MS with help from DH.

In paper 5, the a priori tests were performed by MS, while the model predictions were performed by Wallin (SW). The theoretical work and writing was done by MS and SW together.

The Couette data were produced and evaluated by Komminaho (JK) in paper 6. The boundary layer data were produced and evaluated by MS. JK wrote the part about the Couette flow, while the part about the boundary layer was written by MS.

Haritonidis (JH) came up with the original idea for the work in paper 7. The simulations were performed by MS and JH together. The stability analysis was performed by MS with a lot of help from JH and DH. The paper was written by MS with help from JH and DH.

The work described in paper 8 was performed by Alvelius and MS together. It was also written together.

MS contribution in paper 9 was the pressure solver and to compile and organize the report.

Contents

"A dry maple leaf fell off and is dropping to the ground; its movement is exactly like the flight of a butterfly. Isn't it strange? The most mournful and dead—resembles the most gay and lively."

Ivan Turgenev

CHAPTER 1

Introduction

The phenomenon leading to such an exclaim of wonder as on the previous page is caused by the motion of air, which mysteries are investigated in the field of fluid mechanics.

Actually, there is no mystery at all. Newton's second law of motion and a constitutive relation regarding the viscous forces describe the motion in mathematical terms (equations). The equations are called Navier-Stokes (N-S) equations and form together with the continuity equation (conservation of mass) a system of four equations for the four variables: velocity vector (three components) and pressure. However, because the flow can be complicated enough to even resemble living things, it is difficult to solve the governing equations. In other words, the flow is represented by a simple equation (when put in a mathematical formulation), but the solution may not be simple. Only very special solutions to the N-S equations can be solved mathematically to a closed expression, i.e. the velocity vector given as a function of time and space. For more realistic situations, the solution has to be calculated with the aid of a computer. Alternatively, experiments have to be conducted to extract information about the flow.

Most of the flows in nature and in technical applications are turbulent, i.e. the velocity fluctuates rapidly in time and space. This is what makes the dry leaf come to life. Other examples include the flow over the wing of an aircraft and the flow of blood through our veins.

To numerically solve the N-S equations is called direct numerical simulation (DNS) and is an enormous challenge for the super computers in use today. The difficulties that arise when performing DNS are due to the wide range of scales in the turbulence that need to be resolved, making the simulations large and time consuming. By scales one means the lengths (both in time and space) that are important for the dynamics of the flow. The large scales are determined by the outer, geometrical constraints, and the smallest scales are determined by the viscosity (inner friction). The range of scales is measured by the Reynolds number.

Another example of the complexity of fluid motion, actually involving a butterfly, is that the flap of such tiny wings might be responsible for a full storm on the other side of the earth. This illustrates another difficulty in the prediction of fluid flows; the sensitivity to changes in boundary conditions

or initial conditions, which manifests itself in, among other things, the large uncertainty in weather forecasts.

The usual concept in research of physical phenomena is to translate the physics to mathematics, then solve the mathematical problem, and finally translate the answer back to physics. The construction of a mathematical model of the physical reality usually requires some assumption about the physics — a simplification, or at least an interpretation of nature. In the part of fluid mechanics dealt with here, the assumptions are

i the continuum hypothesis; the molecules are so small and many that they constitute a continuum. This is the basis of fluid mechanics, and will not be further discussed.

ii the incompressibility of fluid; the density of the fluid is constant. The work presented here concerns flow at relatively low speed, thus compressibility is of no concern.

iii Newtonian fluid; the relationship between the stresses and the rates of deformation is linear. The work presented here concerns air or water, which are Newtonian fluids.

A physical experiment is the natural method for extracting information about fluid flows. Why would one want to perform a numerical simulation? There is a number of advantages with DNS over experiments. The most obvious ones include the information of the flow close to the wall, which is crucial in many aspects. It is difficult to measure close to the surface, while the full information is available from numerical data. Furthermore, to have access to all flow variables at the same instant is important in turbulence research, and is only possible with numerical simulations.

However, because the limited performance of computers, DNS is constrained to simple geometries and low Reynolds numbers. Thus, DNS is only suitable for basic studies of turbulence.

From an engineering point of view, the information needed for the design consists of the average of the turbulent flow. Therefore, the full N-S equations describing every detail in time and space are not necessary, or even desirable, to solve. It is sufficient to solve the equations for the averaged flow, which are obtained by taking the time or ensemble average of the full N-S equations. The equations describing the mean flow have terms included that describe the influence of the fluctuating part of the velocity on the mean. These terms are unknown and must be modelled, i.e. they need to be expressed in the mean flow variables. A lot of research has been devoted to this so called turbulence modelling. All of the numerical calculations of turbulent flows of engineering interest are performed using turbulence models.

The flow around an object that moves in air or water is responsible for such phenomena as drag and lift. Close to a solid surface the flow forms a boundary layer, where the speed of the fluid relative the object rapidly decreases to zero. In this relatively thin layer many of the most interesting features of the aerodynamic property of the body are determined. Thus, the boundary layer is of engineering significance in most applications. Furthermore, the flow within

this boundary layer is often turbulent. This type of flow, called turbulent boundary layer flow, is the topic of this thesis.

In this thesis some features of the flow are compared with theoretical expressions, obtained from the averaged N-S equations (Reynolds equations), or more specifically, a simplified version (the turbulent boundary layer equation). The motivation for the theoretical work is to explain the behaviour of the mean flow of the turbulent boundary layer. Furthermore, relating the DNS data with theoretical results give an opportunity to advance turbulence models further than is possible if only comparisons between DNS data and model predictions are made.

References to papers 1 through 9 will be made in the following chapters. The papers are included in the thesis and the proper reference is stated in the preface.

Direct numerical simulation

2.1. Numerical method

The direct numerical simulations presented in this thesis have all been performed with the spectral algorithm described in detail in paper 9. In a spectral method the solution is approximated by an expansion in smooth functions, e.g. trigonometric functions as in our case. The earliest applications to partial differential equations were developed by Kreiss & Oliger (1972) and Orszag (1972), who named the method pseudo-spectral. The term pseudo-spectral refers to the multiplications in the non-linear terms, which are calculated in physical space to avoid the evaluation of convolution sums. The transformation between physical and spectral space can be efficiently done by Fast Fourier Transform (FFT) algorithms that became generally known in the 1960's, see Cooley & Tukey (1965).

The high accuracy in spectral methods compared to finite-element or finite difference discretizations is a result of the fast convergence rate of spectral approximations of a function. Efficient implementations of pseudo-spectral methods can be made thanks to the low costs of performing FFTs. Moreover, the data structure makes the algorithms suitable for both vectorization and parallelization. However, the spectral approximation limits the applications to simple geometries.

Pseudo-spectral methods became widely used for a variety of flows during the 1980's. Early turbulent boundary layer results were presented by Spalart & Leonard (1987), who used a parallel approximation of the boundary layer. The first spatial (no parallel approximation) turbulent boundary layer computation was performed by Spalart & Watmuff (1993).

The algorithm used for the simulations in this thesis is similar to that for channel geometry of Kim *et al.* (1987), using Fourier series expansion in the wall parallel directions and Chebyshev series in the normal direction and pseudo-spectral treatment of the non-linear terms. The time advancement used is a four-step low storage third-order Runge-Kutta method for the non-linear terms and a second-order Crank-Nicolson method for the linear terms. Aliasing errors from the evaluation of the non-linear terms are removed by the $3/2-$rule when the horizontal FFTs are calculated.

The numerical code is written in FORTRAN and consists of two major parts; one linear part where the equations are solved in spectral space, and one non-linear part where the non-linear terms in the equations are computed in
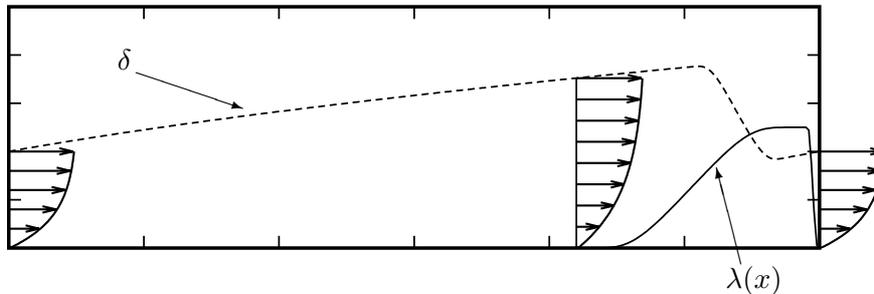
FIGURE 2.1. The boundary layer thickness δ (dashed) of a laminar mean flow that grows downstream in the physical domain and is reduced in the fringe region by the forcing. The flow profile is returned to the desired inflow profile in the fringe region, where the fringe function $\lambda(x)$ is non-zero.

physical space. The linear part needs data for one spanwise (z) position at a time since the equations are solved in the wall normal (y) direction. The non-linear part needs data for one y position at a time since the FFT is performed in the horizontal directions (spanwise and streamwise). The flow variables are stored at an intermediate level with spectral representation in the horizontal directions and physical representation in the y direction. All spatial derivatives are calculated with spectral accuracy. The main computational effort in these two parts is in the FFT.

Since the boundary layer is developing in the downstream direction, it is necessary to use non-periodic boundary conditions in the streamwise direction. This is possible while retaining the Fourier discretization if a fringe region, similar to that described by Bertolotti *et al.* (1992), is added downstream of the physical domain. In the fringe region the flow is forced from the outflow of the physical domain to the inflow. In this way the physical domain and the fringe region together satisfy periodic boundary conditions. The fringe region is implemented by the addition of a volume force F, to the Navier-Stokes equations:

$$\frac{\partial u_i}{\partial t} + u_j \frac{\partial u_i}{\partial x_j} = -\frac{1}{\rho}\frac{\partial p}{\partial x_i} + \nu \frac{\partial^2 u_i}{\partial x_j{}^2} + F_i. \tag{2.1}$$

The force

$$F_i = \lambda(x)(\tilde{u}_i - u_i) \tag{2.2}$$

is non-zero only in the fringe region; $\tilde{u}_i$ is the laminar inflow velocity profile the solution u_i is forced to and $\lambda(x)$ is the strength of the forcing. The form of $\lambda(x)$ is designed to minimize the upstream influence. See Nordström *et al.* (1999) for an investigation of the fringe region technique. Figure 2.1 illustrates

the variation of the boundary layer thickness and the mean flow profile in the computational box for a laminar case, as well as a typical fringe function $\lambda(x)$.

The code has been thoroughly checked and used in several investigations by a number of users on a variety of workstations and super computers.

2.2. Computer implementation

Many super computers of various types have been used for the simulations. All of the computers have been parallel, i.e. multiple processors are working together at the same time. The computers can be divided in two groups with respect to processor type, and two groups with respect to memory configuration.

A processor has either scalar or vector registers. A scalar processor performs operations on one element at a time with fast access to memory, whereas a vector processor performs operations on several elements at the same time.

The processors can have access to a large memory, common to all processors (shared memory), or have their own memory, unique for all processors (distributed memory).

All combinations of the different types have been used and the computers are listed in table 2.1.

	shared memory	distributed memory
scalar processor	SGI Origin 200	Cray T3E, IBM SP2
vector processor	Cray J90, C90, T90	Fujitsu VPP300, NWT

TABLE 2.1. The four categories of super computers

While the parallelization of the code on shared memory computers is straightforward, a lot of effort was needed for the parallelization and optimization of the code on computers with distributed memory, see paper 8. Communication between processors is necessary when the operations on the data set are to be performed in the two different parts of the code. The data set (velocity field) is divided between the different processors along the z direction. Thus, in the linear part, no communication is needed. When the non-linear terms are calculated, each processor needs data for a horizontal plane. The main storage is kept at its original position on the different processors. In the non-linear part each processor collects the two dimensional data from the other processors, on which it performs the computations, and then redistributes it back to the main storage.

The tuning of a code for optimal performance consists of two parts. One is the single processor tuning and the other is the parallel optimization. The tuning for one processor is dependent on the type of processor, whereas the parallelization is connected to the memory configuration. The two main issues for the single processor performance are the vectorized versus scalar FFT. For the parallelization the inherent structure of the code makes it suitable for shared

memory systems, and for distributed memory the MPI (Message-Passing Interface) is utilized.

An overview of the performance on the different computers used for the simulations presented in this thesis is shown in table 2.2. The peak performance in the table is the theoretical maximum speed you could obtain on a single processor. This number is more closely obtained in reality for vector processors. Note that the clock frequency usually quoted in connection with personal computers is somewhat misleading in this context. The clock frequency for e.g. the SP2 processor is only 160 MHz, but it is capable of four operation in each clock cycle, making the top performance 640 million floating point operations per second (640 Mflop/s).

The largest computer used for the simulations was the Numerical Wind Tunnel (NWT) at the National Aerospace Laboratory (NAL), Tokyo. It was built in the early 90's and consists of 166 vector processors from Fujitsu.

Computer	# processors	peak performance	code performance
Cray J90	1	220	100^1
Cray J90	8		600
Cray C90	1	952	522^1
Cray C90	4		1500
Cray T90	1	1700	710
Fujitsu VPP300	1	2200	525
Fujitsu NWT	1	1700	320^2
Fujitsu NWT	64		20500
Cray T3E	1	600	30^2
Cray T3E	64		1900
IBM SP2	1	640	55^2
IBM SP2	64		3500
SGI Origin 200	1	450	53
SGI Origin 200	4		181

TABLE 2.2. The speed on various super computers in Mflop/s.
[1] Measured with optimal vector length, same performance not possible on several processors. [2] Not measured, but calculated from performance on 64 processors for comparison.

2.3. Performed simulations

The adverse pressure gradient is implemented through the variation of the streamwise velocity at the freestream (U). In all of the simulations presented in this thesis the form of U has been,

$$U = U_0(1 - \frac{x}{x_0})^m. \tag{2.3}$$

Both the exponent m and the virtual origin x_0 are parameters defining the shape of U. The parameters used in the simulations are given in table 2.3.

The simulations start with a laminar boundary layer at the inflow which is triggered to transition by a random volume force near the wall. All the quantities are non-dimensionalized by the freestream velocity (U) and the displacement thickness (δ^*) at the starting position of the simulation ($x = 0$), where the flow is laminar. The Reynolds number is set by specifying $Re_{\delta^*} = U\delta^*/\nu$ at $x = 0$, and the values are given in table 2.3. The length (including the fringe), height and width of the computational box are listed in table 2.3 together with the number of modes used. Also included in table 2.3 are the total number of collocation points, denoted N_c.

Case	Re_{δ^*}	L_x	L_y	L_z	N_x	N_y	N_z	N_c	m	x_0
ZPG	450	600	30	34	640	201	128	$37 \cdot 10^6$	0	∞
A1	400	450	18	24	480	121	96	$13 \cdot 10^6$	-0.077	-60
A2	400	450	24	24	480	161	96	$17 \cdot 10^6$	-0.15	-60
A3	400	700	65	80	512	193	192	$43 \cdot 10^6$	-0.25	-62
SEP	400	700	65	80	720	217	256	$90 \cdot 10^6$	-0.35	-50

TABLE 2.3. Numerical parameters. L denotes the size of the computational box. N denotes the number of modes.

The five different simulations are presented in six of the nine papers included in this thesis, as well as in a number of conference proceedings not included. The simulations have different notations in the papers and are summarized in table 2.4.

Thesis	paper 1	paper 2	paper 4	paper 5	paper 6	paper 7
ZPG					ZPG	ZPG
A1	APG1	APG1				
A2	APG2	APG2			APG1	
A3			APG1	APG1	APG2	
SEP			SEP	SEP		

TABLE 2.4. The simulations are presented in different papers with a notation summarized here.

CHAPTER 3

Fundamental analysis of turbulent boundary layer flows

In most applications it is the mean flow that sets the limit on the performance and hence determines the design. The rapid turbulent fluctuations in time and space are not in themselves as interesting as their influence on the time-averaged flow. The equations to be solved to obtain the steady mean flow is the averaged Navier-Stokes equations (Reynolds equations),

$$\frac{\partial u_i}{\partial x_i} = 0, \tag{3.1}$$

$$u_j \frac{\partial u_i}{\partial x_j} = -\frac{1}{\rho}\frac{\partial P}{\partial x_i} + \nu\frac{\partial^2 u_i}{\partial x_j{}^2} - \frac{d}{dx_j}\langle u_i' u_j'\rangle, \tag{3.2}$$

where $\langle u_i' u_j'\rangle$ is the Reynolds stress tensor, which is the quantity that accounts for the influence of the turbulent fluctuations on the mean flow u_i. P is the mean pressure.

By solving equation (3.2), the mean flow u_i is obtained. However, $\langle u_i' u_j'\rangle$ is an unknown quantity that needs to be expressed in u_i and its derivatives in order to obtain a solvable equation. Thus, one objective for DNS is to obtain turbulence statistics from which the true coupling between mean flow and Reynolds stresses can be extracted. From the results it is possible to draw conclusions about the validity of current turbulence models and also to develop new models. Furthermore, the solution to equation (3.2) does not contain any information about the instantaneous flow. However, for the coupling between the mean flow and Reynolds stresses, the instantaneous structure of the flow could be of importance.

3.1. The boundary layer equations
In a steady two-dimensional boundary layer the mean flow equations (3.1) and (3.2) reduce to,

$$\frac{\partial u}{\partial x} + \frac{\partial v}{\partial y} = 0, \tag{3.3}$$

$$u\frac{\partial u}{\partial x} + v\frac{\partial u}{\partial y} = -\frac{1}{\rho}\frac{dP}{dx} + \nu\frac{\partial^2 u}{\partial y^2} - \frac{\partial}{\partial y}\langle u'v'\rangle - \frac{\partial}{\partial x}\left(\langle u'u'\rangle - \langle v'v'\rangle\right), \tag{3.4}$$

where u is the mean streamwise velocity, v the mean wall normal velocity, $\frac{dP}{dx}$ the pressure gradient, $\langle u'v'\rangle$, $\langle u'u'\rangle$, $\langle v'v'\rangle$ the Reynolds stresses, ρ the

density and ν the kinematic viscosity. Equation (3.4) is the turbulent analogy to the laminar second order boundary layer approximation, i.e. terms up to order $(\delta/L)^2$ are kept, where δ is a typical length in the normal direction and L is a typical length in the streamwise direction. The last term in equation (3.4) can be neglected in most situations, and the resulting equation is a first order boundary layer approximation. This simplified turbulent boundary layer equation will be denoted TBLE throughout this chapter. The TBLE can be further simplified by the distinction between an inner part and an outer part.

3.2. Scalings and self-similarity

One important concept in the analysis of equation (3.4) is self-similarity, which means that velocity profiles at different downstream positions collapse on a single curve. In order to achieve this, proper scaling has to be used.

The concept of scaling and self-similarity has been an important tool in physics for a long time. According to Barenblatt (1996), the first application was made by Fourier (1822), in the context of heat conduction.

By reducing a partial differential equation — with two or more independent variables, to an ordinary equation — with one independent variable, an enormous simplification of the problem has been made.

The velocities and Reynolds stresses in equation (3.4) are dependent on both x and y. However, under certain conditions the dependency can be reduced to only one *similarity* coordinate (which depends on x and y).

In turbulent boundary layer theory one usually distinguish between two regions of the flow with different characteristics. The individual terms in equation (3.4) are of different importance in the two regions of the boundary layer flow. The viscous term is only important in the inner region, while the advection terms are only significant in the outer part.

3.2.1. *The outer part*

In the outer part of a turbulent boundary layer, equation (3.4) can be reduced to,

$$u\frac{\partial u}{\partial x} + v\frac{\partial u}{\partial y} = -\frac{1}{\rho}\frac{dP}{dx} - \frac{\partial}{\partial y}\langle u'v'\rangle. \tag{3.5}$$

The partial differential equation (3.5) is converted to an ordinary differential equation through the rescaling,

$$
\begin{aligned}
(u - U)/u_\tau = F(\eta), & \qquad -\langle u'v'\rangle/u_\tau{}^2 = R(\eta), \\
\eta = y/\Delta(x), & \qquad \Delta = U\delta^*/u_\tau.
\end{aligned} \tag{3.6}
$$

U is the freestream velocity, u_τ is the friction velocity (defined in the next section) and δ^* is the displacement thickness. These scalings yields an equation of the form,

$$-(\beta - 2\omega)F + \gamma F^2 - (\alpha - 2\beta - 2\omega)\eta\frac{dF}{d\eta} - \chi\frac{dF}{d\eta}\int_0^\eta F d\eta = \frac{dR}{d\eta}, \tag{3.7}$$

with

$$\alpha = \left(\frac{U}{u_\tau}\right)^2 \frac{d\delta^*}{dx}, \ \beta = \frac{\delta^*}{\tau_w}\frac{dp}{dx}, \tag{3.8}$$

$$\omega = \frac{1}{2}\frac{\delta^*}{u_\tau}\left(\frac{U}{u_\tau}\right)^2 \frac{du_\tau}{dx},$$

$$\gamma = \frac{U}{u_\tau}\frac{\delta^*}{u_\tau}\frac{du_\tau}{dx}, \ \chi = \frac{U}{u_\tau}\frac{d\delta^*}{dx} + \frac{\delta^*}{u_\tau}\frac{dU}{dx}.$$

If the scalings in (3.6) is to produce an ODE of equation (3.7), all the terms $\alpha, \beta, \gamma, \chi, \omega$ must be constants. The conditions under which constant parameters can occur are discussed next.

The classical treatment of the equations which involves outer and inner equations and a matching of the solutions, leads to the logarithmic friction law,

$$\frac{u_\tau}{U} = \frac{1}{C + \frac{1}{\kappa}\ln Re_{\delta^*}}, \tag{3.9}$$

where κ is the Kármán constant and $Re_{\delta^*} = U\delta^*/\nu$. Equation (3.9) shows that $u_\tau/U \to 0$ in the limit of very high Reynolds number. A series expansion of the terms (3.8) in the small parameter (u_τ/U) is performed in paper 2. Letting $u_\tau/U \to 0$, the asymptotic version of equation (3.7) is obtained,

$$-2\beta F - (1+2\beta)\eta\frac{dF}{d\eta} = \frac{dR}{d\eta}, \tag{3.10}$$

which is called the defect layer equation. The same asymptotic version was obtained by Tennekes & Lumley (1972). Also Wilcox (1993) performed an asymptotic analysis but made some mistakes as pointed out in paper 2 and by Henkes (1998).

A different approach to equation (3.4) is presented in paper 1, in which the asymptotic theory is substituted with an analysis permitting a finite ratio u_τ/U. Since the logarithmic function grows very slowly when the argument is large, a better assumption than $u_\tau/U \to 0$ for moderately high Reynolds numbers is that $u_\tau/U \approx$ constant. If u_τ/U is regarded as constant and an outer length scale varies linearly, the condition $\beta =$constant is fulfilled if the freestream variation is of the form $U \sim x^m$, which was shown by Townsend (1956) and Mellor & Gibson (1966). When specifying a profile in a power-law form it can be written,

$$U = U_0(1 - \frac{x}{x_0})^m. \tag{3.11}$$

Utilizing these constraints, the TBLE becomes,

$$-2\beta F + \frac{\beta}{m}(1+m)\eta\frac{dF}{d\eta}$$

$$+\frac{u_\tau}{U}\left\{-\beta F^2 + \frac{\beta}{m}(1+m)\frac{dF}{d\eta}\int_0^\eta F d\eta\right\} = \frac{dR}{d\eta} + \frac{1}{Re_{\delta^*}}\frac{d^2F}{d\eta^2}. \tag{3.12}$$

If now $u_\tau/U \to 0$, the asymptotic version becomes,

$$-2\beta F + \frac{\beta}{m}(1+m)\eta \frac{dF}{d\eta} = \frac{dR}{d\eta}. \qquad (3.13)$$

The relation between the equations (3.10), (3.12) and (3.13), and what they can be used for is discussed in the next chapter.

3.2.2. *The inner part*

The analysis of the flow near the wall is important because many features of the flow of engineering significance is determined in the near-wall region. In the inner part of a zero pressure gradient boundary layer, equation (3.4) can be reduced to,

$$0 = \nu \frac{\partial^2 u}{\partial y^2} - \frac{\partial}{\partial y}\langle u'v'\rangle. \qquad (3.14)$$

The right hand side is interpreted as the gradient of the shear stress τ (or actually the gradient of τ/ρ), and equation (3.14) can be integrated from the wall to give an expression for τ itself as a function of y and x,

$$\frac{\tau}{\rho} \equiv \nu \frac{\partial u}{\partial y} - \langle u'v'\rangle = \left(\nu \frac{\partial u}{\partial y} - \langle u'v'\rangle \right) \bigg|_{y=0} \qquad (3.15)$$

The Reynolds stress is zero at the wall and we define the friction velocity u_τ as,

$$u_\tau \equiv \sqrt{\nu \frac{\partial u}{\partial y}\bigg|_{y=0}}. \qquad (3.16)$$

If we use the viscous scaling (or plus units); $u^+ \equiv u/u_\tau$, $y^+ \equiv yu_\tau/\nu$ and $\tau^+ \equiv \tau/(\rho u_\tau^2)$, equation (3.15) can be written,

$$\tau^+ \equiv \frac{du^+}{dy^+} - \langle u'v'\rangle^+ = 1, \qquad (3.17)$$

which implies that all the dependency on x is included in u_τ. The assumption that u^+ is a function of only y^+ was first made by Prandtl (1932). In the viscous sub-layer, where the Reynolds stress is negligible, equation (3.17) can be integrated to yield $u^+ = y^+$, i.e. the velocity profile is a function of only one variable, which in turn depends on both x and y.

Equation (3.17) with the pressure gradient term included can be written as,

$$\tau^+ = 1 + \left(\frac{u_p}{u_\tau} \right)^3 y^+, \qquad (3.18)$$

with

$$u_p \equiv \left(\nu \frac{1}{\rho} \frac{dP}{dx} \right)^{1/3}. \qquad (3.19)$$

The linear behavior of the total shear stress revealed in equation (3.18) was first observed by Stratford (1959*a,b*).

In the viscous sub-layer the Reynolds shear stress approaches zero and equation (3.18) can be integrated to give,

$$u^+ = y^+ + \frac{1}{2}\left(\frac{u_p}{u_\tau}\right)^3 (y^+)^2. \tag{3.20}$$

This equation was first derived by Patel (1973), and reduces to the usual linear profile in ZPG case, when $u_p \to 0$.

It can be shown that the pressure gradient term decreases with increasing Reynolds number. The term is thus important only for low Reynolds numbers. However, close to separation, where u_τ approaches zero, it is clear that the terms becomes infinite, even for large Reynolds numbers.

For the ZPG case, the scaling of the total shear stress with u_τ gives a self-similar profile ($\tau^+ = 1$). From equation (3.18) it is observed that the velocity scale u_τ does not results in a self-similar expression. However, equation (3.18) can be formulated as

$$\tau^* \equiv \frac{1}{u_*^2}\left(\nu\frac{\partial u}{\partial y} - \langle u'v' \rangle\right) = 1, \tag{3.21}$$

where u_* is a velocity scale that depends on y and can be expressed as

$$u_*^2 = u_\tau^2 + \frac{u_p^3}{u_\tau}y^+. \tag{3.22}$$

The only velocity scale in the inner part of the ZPG boundary layer is u_τ. By normalizing the velocity gradient with y and u_τ, and assume this scaling leads to a constant non-dimensional velocity gradient for large enough y^+, (see e.g. Bradshaw & Huang (1995)), we get the equation,

$$\frac{y}{u_\tau}\frac{\partial u}{\partial y} = \frac{1}{\kappa}. \tag{3.23}$$

When expressed in inner scales and integrated, equation (3.23) yields the logarithmic velocity profile.

In the APG boundary layer, the velocity scale is u_*, and using this velocity scale in the normalization of the velocity gradient yields,

$$\frac{y}{u_*}\frac{\partial u}{\partial y} = \frac{1}{\kappa}. \tag{3.24}$$

When expressed in inner scales and integrated, equation (3.24) yields,

$$u^+ = \frac{1}{\kappa}\left(\ln y^+ - 2\ln\frac{\sqrt{1+\lambda y^+}+1}{2} + 2(\sqrt{1+\lambda y^+}-1)\right) + B, \tag{3.25}$$

with

$$\lambda = \left(\frac{u_p}{u_\tau}\right)^3.$$

A more thorough derivation of equation (3.25) is given in paper 4. Townsend (1961), Mellor (1966) and Afzal (1996) have derived similar equations, albeit with different methods and assumptions. Equation (3.25) will be compared

with DNS data in the next chapter where also the corresponding equation for the separated boundary layer will be presented.

CHAPTER 4

Turbulent boundary layers under adverse pressure gradients

The turbulent boundary layer under an adverse pressure gradient (APG) is decelerated, which does not mean that the turbulence intensity decreases. On the contrary, the flow becomes even more unstable and the turbulence activity is enhanced. The boundary layer also grows (thickens) more rapidly under the influence of an APG. Since the momentum of the fluid is lower close to the wall than further up in the boundary layer, the flow near the wall is more severely affected by the pressure gradient. If the pressure gradient is strong enough, the flow close to the wall separates, i.e. reversed flow appears.

4.1. General features

In figure 4.1 the freestream velocity (U) for all five simulations included in this thesis are shown. These profiles constitute the boundary condition on the upper edge of the computational box and define the APG. The resulting skin friction ($C_f \equiv 2(u_\tau/U)^2$) of the four attached boundary layers are shown in figure 4.2. As the APG is increased the C_f is reduced. If the APG is strong enough it induces separation ($C_f < 0$), which occurs for the freestream distribution used in the case SEP. The C_f for SEP is shown in figure 4.3, where also the C_f distributions for previously completed simulations of a separated turbulent boundary layer are included. The two earlier simulations were performed by Na & Moin (1998) and Spalart & Coleman (1997). In figure 4.3 the x values have been recalculated in our simulation coordinates. However, the relative starting positions of the boundary layers cannot be calculated and are here matched by letting the starting points of all three simulations be located at $x = 0$. From figure 4.3 it is clear that the separation bubble is longer in the present simulation (case SEP) than in the other two. In figure 4.3 the C_f from our simulation has been calculated using the same technique as in Na & Moin (1998) and Spalart & Coleman (1997), i.e. with a value of unity for the freestream velocity. More results from the separated boundary layer simulation are presented in section 4.4.

The streamwise velocity profile at $x = 300$ is shown for the five cases in figure 4.4. The simulations were performed with different heights of the computational box, as seen in figure 4.4. The heights in A3 and SEP were actually 65 but the profiles are shown up to 45. The freestream velocity is unity
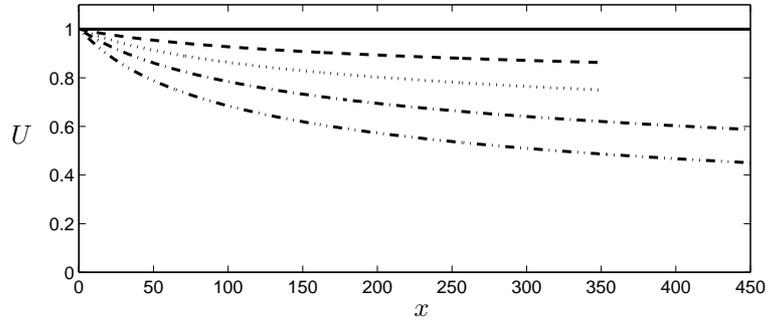
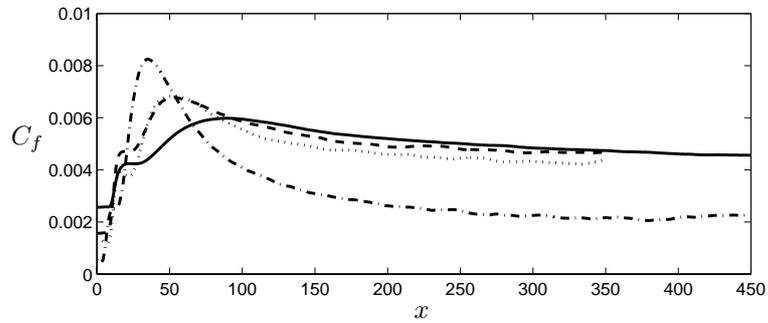FIGURE 4.1. U. — ZPG; - - A1; $\cdots$ A2; $- \cdot -$ A3; $- \cdot \cdot -$ SEP.

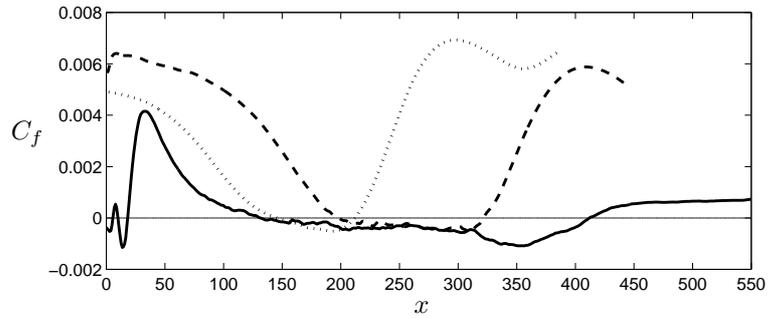FIGURE 4.2. C_f. — ZPG; - - A1; $\cdots$ A2; $- \cdot -$ A3.

FIGURE 4.3. — C_f from SEP; - - C_f from Na & Moin (1998); $\cdots$ C_f from Spalart & Coleman (1997).

only for ZPG. The profile from SEP exhibits negative values of the velocity close to the wall, showing that separation has occurred.

The streamwise velocity fluctuations form elongated structures near the wall in a ZPG boundary layer. It is generally thought that the structures are weakened in an APG flow. This is illustrated in figure 4.5, where the streamwise
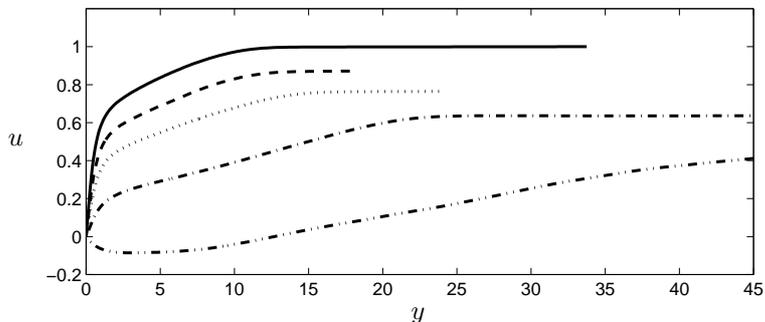
FIGURE 4.4. Streamwise velocity profiles at $x = 300$. — ZPG; - - A1; $\cdots$ A2; $-\cdot-$ A3; $-\cdot\cdot-$ SEP.

velocity fluctuations in a horizontal plane from ZPG, A3 and SEP are shown. The figure shows the whole computational boxes in the spanwise direction and excluding the transitional part and fringe region in the streamwise direction. The dark color represents the low-speed regions and light color represents the area containing high-speed fluid. The streaks formed in the ZPG case (figure 4.5a) are spaced 100 viscous units in the spanwise direction. The streaks in the A3 case are shown in figure 4.5b. The structures are weakened at the end of the domain as compared with those in the beginning, showing the damping effect of the APG on the structures. The spacing between the structures increases from 100 (the same as for a ZPG layer) at the beginning to about 130 at the end, based on the local u_τ.

The SEP case is shown in figure 4.5c. There are still some structures in the separated flow, though not at all as long and frequent as in the ZPG or A3. Before separation, which occurs at approximately $x = 142$, the streaks are visible, but are rapidly vanishing in the beginning of the separated region. There is notable increase in the streak formation around $x = 350$, where the friction coefficient is at its lowest values, c.f. figure 4.3. Thus, there are indications that streaks may reappear in a separated region if the back flow is severe enough. After the reattachment at $x = 412$ the streaks are not immediately appearing, but are clearly visible after $x = 450$.
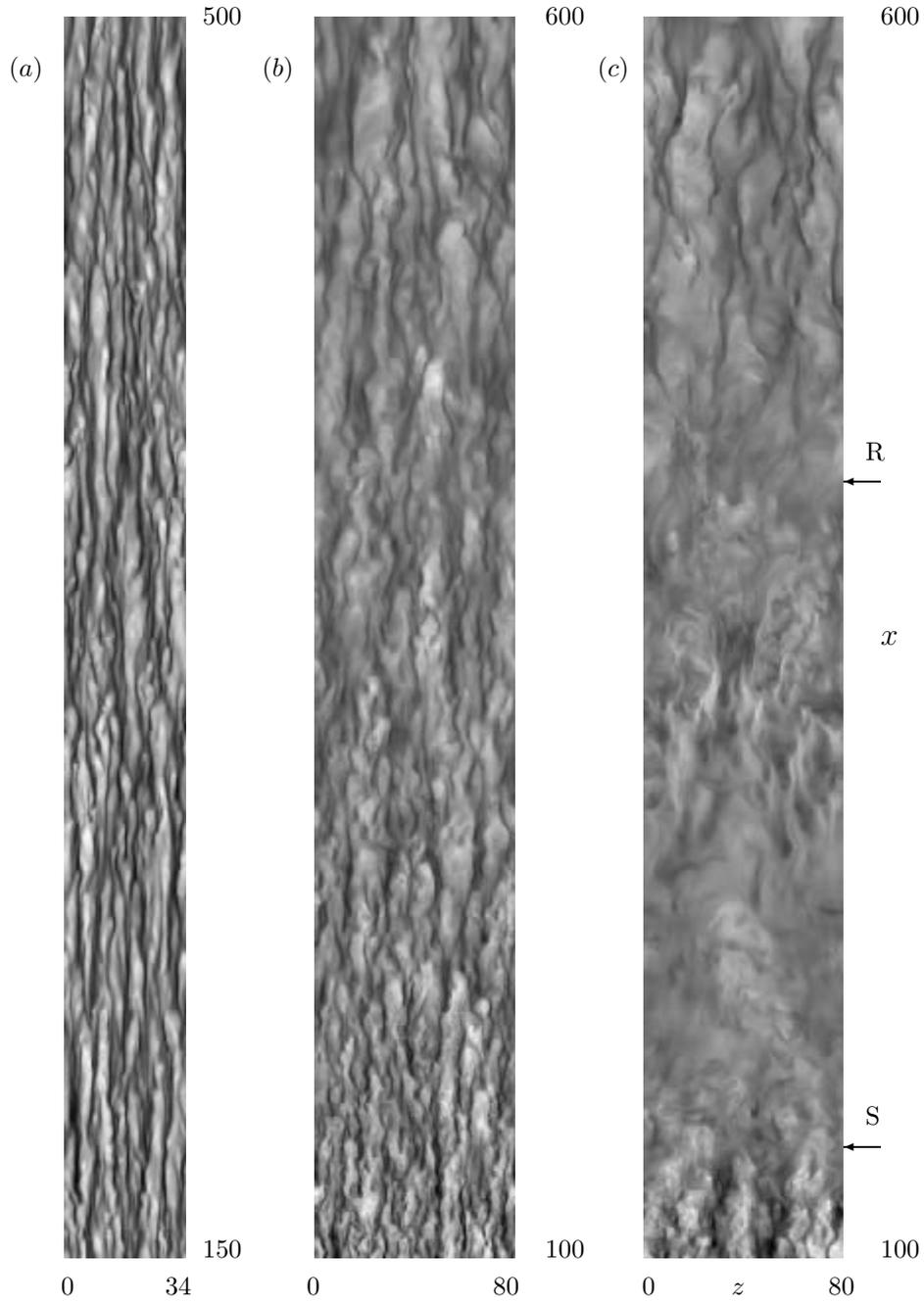
FIGURE 4.5. Streamwise velocity fluctuations in a horizontal plane at $y^+ = 10$. (a) ZPG. (b) A3. (c) SEP. The points denoted S and R represent the separation and reattachment respectively.

4.2. The outer region of the boundary layer

4.2.1. *Self-similarity*

The simulations presented in paper 1 showed constant β, see table 4.1. However, the functions $F(\eta)$ and $R(\eta)$ are not self-similar for low Reynolds numbers as shown with DNS in paper 1. For large Reynolds numbers, the functions $F(\eta)$ and $R(\eta)$ do become self-similar and converge to the asymptotic defect layer equation given be equation (3.10), as shown with turbulence models in paper 2 and by Henkes (1998).

The shapes of $F(\eta)$ from the simulations are shown in figure 4.6. The β parameter has a strong influence on the profile shape for A3, while the A1 and A2 profiles are closer to the ZPG profile.
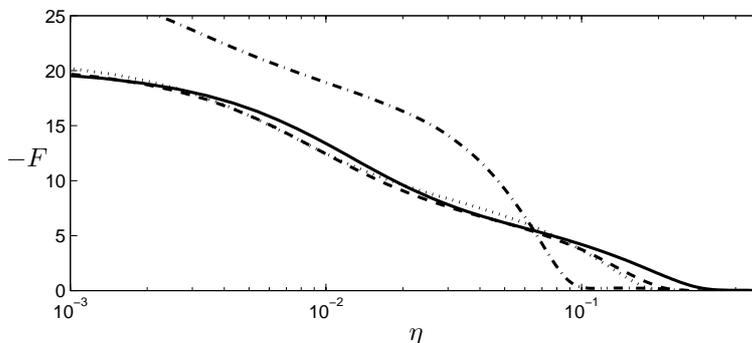

FIGURE 4.6. Velocity profiles at $x = 300$. — ZPG; - - A1; $\cdots$ A2; $- \cdot -$ A3.

4.2.2. *Mean flow parameters*

The equation describing the outer region can be integrated from the wall to the freestream, and thereby provide relations between mean flow parameters. If equation (3.13) is integrated, the relation

$$m = -\frac{\beta}{1 + 3\beta} \tag{4.1}$$

is obtained, and when put back in equation (3.13), equation (3.10) is recovered.

When integrating equation (3.10) it should be noted that the wall boundary condition is $R(0) = 1$ and not $R(0) = 0$. The reason for this is that the near-wall region is neglected when $u_\tau/U \to 0$.

The non-linear equation (3.12) can also be integrated and yields the relation,

$$m = -\frac{\beta}{H(1 + \beta) + 2\beta}, \tag{4.2}$$

where H is the shape factor. The limit $u_\tau/U \to 0$, can now be obtained by letting $H \to 1$, and the relation (4.1) is recovered from (4.2).

To compare the relations (4.1) and (4.2), a number of experiments and DNS are summarized in table 4.1. There is obviously a much better agreement with the non-linear theory, showing that even in high Reynolds number experiments, the asymptotic expressions are of limited value.

The more rapidly U is decreased, the lower C_f is obtained, as shown in figures 4.1 and 4.2. While the relative difference in U between the cases remains the same, a dramatic decrease in C_f occurs between A2 and A3. In other words, the closer to separation the boundary layer is, the more sensitive on the freestream velocity distribution it is. The relation between m and β should reveal this behavior. That so is the case is seen from figure 4.7, where equation (4.2) has been plotted for the two values of H, between which separation has been observed to occur. The limiting value of m increases with H but is confined between -0.22 and -0.25, which is consistent with the observed values in experiments and DNS. The rapid and strongly non-linear approach to separation ($\beta \to \infty$) is consistent with the strong decrease in C_f between A2 and A3 in figure 4.2.

Case	β	H	m	$m = -\frac{\beta}{H(1+\beta)+2\beta}$	$m = -\frac{\beta}{1+3\beta}$
A1	0.24	1.60	-0.077	-0.097	-0.14
A2	0.65	1.63	-0.15	-0.16	-0.22
A3	4.5	1.97	-0.23	-0.23	-0.31
Bradshaw 1	0.9	1.4	-0.15	-0.20	-0.24
Bradshaw 2	5.4	1.54	-0.255	-0.26	-0.31
Skåre & Krogstad	20.0	2.0	-0.22	-0.24	-0.33
Elsberry	25.0	2.45	-0.22	-0.22	-0.33
Stratford	∞	2.5	-0.23	-0.22	-0.33
Spalart & Leonard	1.8	1.65	-0.21	-0.22	-0.28
	8.0	1.92	-0.23	-0.24	-0.32
	∞	2.3	-0.22	-0.23	-0.33
	0.9	1.55	-0.18	-0.19	-0.24
	5.4	1.86	-0.24	-0.24	-0.31

TABLE 4.1. Comparison of m from the non-linear/linear theory. The data are taken from the following references (from top to bottom) Bradshaw (1967), Skåre & Krogstad (1994), Elsberry *et al.* (2000), Stratford (1959a), Spalart & Leonard (1987).

4.3. The inner part of the boundary layer

4.3.1. *The viscous sub-layer*

Profiles in the viscous scaling are compared for the different APG cases in figure 4.8. All of them matches closely the linear profile $u^+ = y^+$. Thus, even
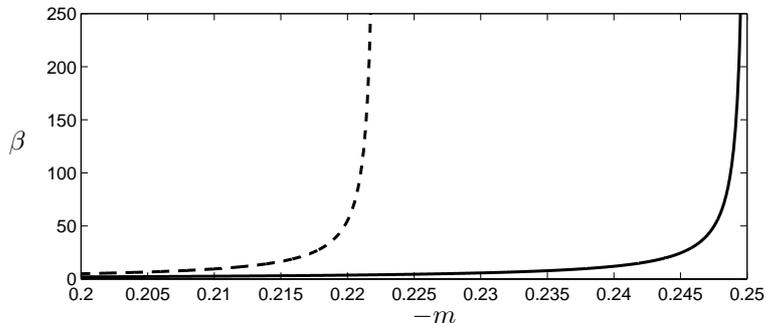
FIGURE 4.7. β as a function of m from equation (4.2) for
— H=2.0 and - - H=2.5.

under strong APG the inclusion of the pressure gradient term does not seem
to be of importance. However, close to separation or reattachment, when u_τ is
small, the velocity profile is strongly influenced by the pressure gradient term.
In figure 4.9, a velocity profile from the SEP case (in the attached region)
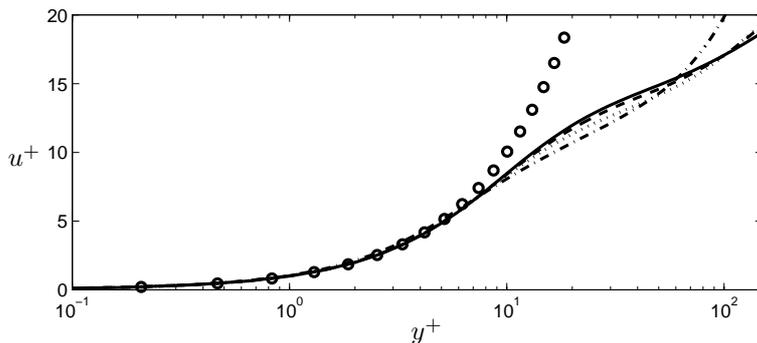illustrates the importance of the pressure gradient term.

FIGURE 4.8. Velocity profiles at $x = 300$. — ZPG; - - A1;
$\cdots$ A2; $-\cdot-$ A3; $\circ$ $u^+ = y^+$.

4.3.2. *The overlap region*

An example of comparison between DNS data and equation (3.25) is shown
in figure 4.10. DNS data from the attached region (at $x = 450$) of the case
SEP is shown as a solid line in figure 4.10. The dashed line is equation (3.25)
and the dotted line is the logarithmic law for the ZPG boundary layer. The
value of additive constant is $B = -2$, which is in agreement with the earlier
investigation of the flow just upstream of separation in the simulation of Na &
Moin (1998), see paper 3.

The value of the Kármán constant, κ, has been set to 0.41 throughout
this thesis. Lately, Österlund *et al.* (2000) have shown that the value of the
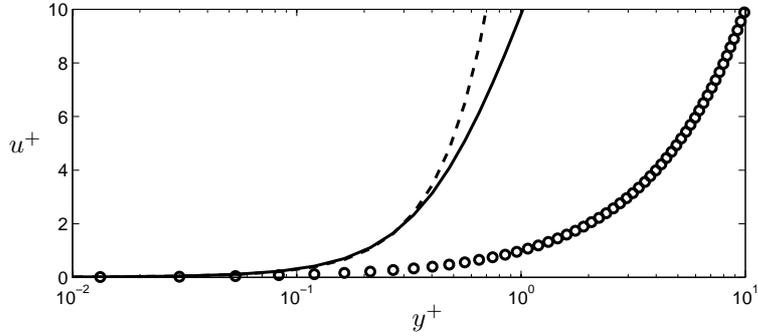
FIGURE 4.9. Velocity profile close to reattachment. — SEP; - - equation (3.20); $\circ$ $u^+ = y^+$.
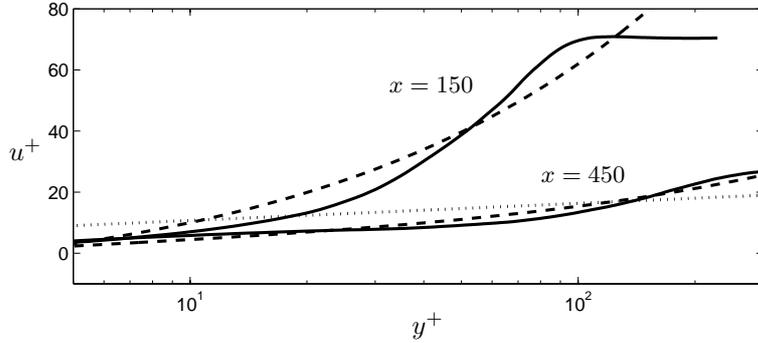

FIGURE 4.10. Velocity profiles from SEP: — DNS; - - equation (3.25) for $x = 450$ and equation (4.8) for $x = 150$; $\cdots$ $u^+ = \frac{1}{0.41} \ln y^+ + 5.1$.

Kármán constant actually is 0.38 for large enough Reynolds number. However, Spalart (1988) has shown that the old value of 0.41 gives good agreement for low Reynolds numbers. In a number of earlier investigations the influence of the Reynolds number on the Kármán constant has been debated, see e.g. Simpson (1970).

4.4. Separation

In paper 4, one of the boundary layers was separated for a large portion of the flow. The contours of mean streamwise velocity are shown in figure 4.11 with positive values shown as solid lines and negative as dashed.

At the point of separation the wall shear stress is zero, i.e. $u_\tau = 0$. Thus the scaling with u_τ encounters a singularity. When considering a strong APG or separation, the singularity can be avoided by using the velocity scale u_p instead of u_τ. This was noted by Stratford (1959b), Townsend (1961) and Tennekes & Lumley (1972). By rescaling equation (3.20) the following expression for the
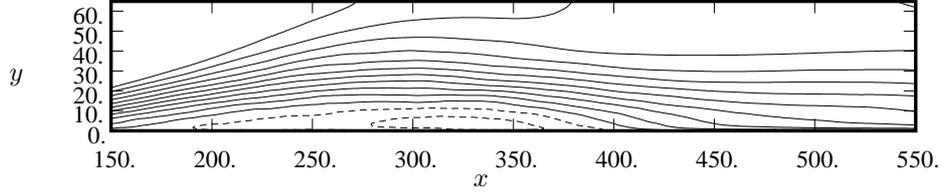
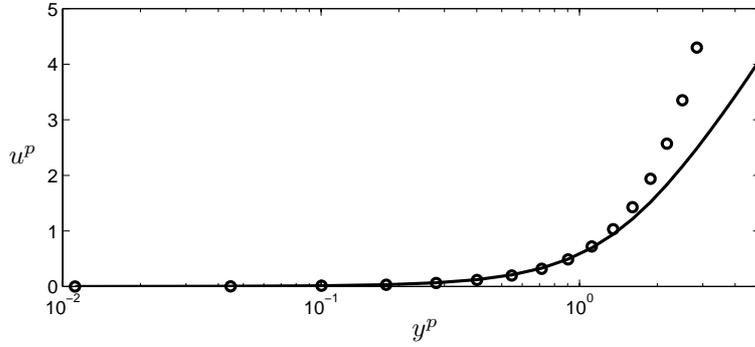FIGURE 4.11. SEP: contours of mean velocity. Positive values shown as solid lines, negative as dashed.

FIGURE 4.12. Velocity profile close to reattachment. — SEP; ○ $u^p = \frac{1}{2}(y^p)^2$.

velocity profile in the viscous sub-layer is obtained,

$$u^p \equiv \frac{u}{u_p} = \frac{1}{2}(y^p)^2 + \left(\frac{u_\tau}{u_p}\right)^2 y^p, \qquad (4.3)$$

where $y^p \equiv y u_p / \nu$. In the limit of separation, when $u_\tau \to 0$, equation (4.3) reduces to

$$u^p = \frac{1}{2}(y^p)^2. \qquad (4.4)$$

Thus, in this rescaled form, the singularity is avoided. The profile from the SEP case at reattachment is shown in figure 4.12 together with the asymptotic expression (4.4). This is the same velocity profile as was shown in figure 4.9. Equation (3.25) can be rewritten in the pressure gradient scaling for the overlap region, and the resulting expression asymptotes to the square-root law when $u_\tau \to 0$,

$$u^p = \frac{1}{\kappa} 2\sqrt{y^p} + C, \qquad (4.5)$$

which was first obtained by Stratford (1959b).

In the separated region the velocity gradient at the wall is negative, and the definition of u_τ needs to be changed to

$$u_\tau \equiv \sqrt{-\nu \frac{\partial u}{\partial y}\bigg|_{y=0}}. \tag{4.6}$$

An integration from the wall was a crucial step in the derivation of the total shear stress. Both the velocity profile in the viscous sub-layer and in the overlap region depends on the expression for the total shear stress. In a separated boundary layer the wall boundary condition is different due to change of sign in the definition of u_τ, which leads to a velocity profile in the viscous sub-layer that reads,

$$u^+ = -y^+ + \frac{1}{2}\left(\frac{u_p}{u_\tau}\right)^3 y^{+2}. \tag{4.7}$$

The velocity profile in the overlap region becomes, in the separated region,

$$u^+ = \frac{1}{\kappa}\left[2\sqrt{\lambda y^+ - 1} - 2\arctan\left(\sqrt{\lambda y^+ - 1}\right)\right] + B, \tag{4.8}$$

with

$$\lambda = \left(\frac{u_p}{u_\tau}\right)^3.$$

One of the profiles (at $x = 150$) from the separated region is shown in figure 4.10 together with the profile given by equation (4.8). The additive constant is $B = -7$ for the separated case. Observe that no part of the back-flow region is shown in figure 4.10. The reader is referred to paper 4 for velocity profiles in the back-flow region.

CHAPTER 5

Modelling of turbulence

The modelling of turbulence can be divided in three major groups. The one we will talk about most is the Reynolds average Navier-Stokes (RANS) modelling. With this expression it is meant that the Reynolds equations are closed by a model for the Reynolds stresses. The second group is large eddy simulation (LES) where the flow is resolved for the large scales while the small scales are modelled. This is completely left out in this work. The third group is the models based on the actual structure of turbulence. The models can e.g. be used for RANS modelling (Perry *et al.* 1994) or for turbulence control purposes.

5.1. RANS modelling

If the mean flow of a turbulent flow is to be calculated by solving the equations (3.1) and (3.2), a relation between the Reynolds stresses and the mean flow is required.

5.1.1. *Basic concepts*

Often the two-dimensional boundary layer is calculated using the equations (3.3) and (3.4) with the last term neglected. Hence, only the Reynolds shear stress needs to be related to the velocity. The simplest relation is the mixing length,

$$-\langle u'v' \rangle^+ = (l^+)^2 \left(\frac{du^+}{dy^+} \right)^2 \qquad \text{with} \qquad l^+ = \kappa y^+, \qquad (5.1)$$

which was first developed by Prandtl (1925). This relation has received a lot of interest during the years and particularly the near-wall behavior of (5.1) is of great importance, even for more sophisticated models. The wall is not naturally accounted for in the relation (5.1), but a successful wall-damping function (f_1) was introduced by van Driest (1956),

$$f_1 = 1 - \exp(-y^+/A^+), \qquad (5.2)$$

which is applied on the mixing length $l^+ = \kappa y^+ f_1$.

The mixing length is based on the concept of turbulent viscosity, first introduced by Boussinesq (1877). The Boussinesq hypothesis can be generalized to the form,

$$a_{ij} = -2 \frac{\nu_T}{K} S_{ij}, \qquad (5.3)$$

where ν_T is the turbulent viscosity. Here we have introduced the anisotropy tensor, $a_{ij} \equiv \langle u_i' u_j' \rangle / K - 2\delta_{ij}/3$, and rate of strain tensor, $S_{ij} \equiv 1/2(U_{i,j} + U_{j,i})$.
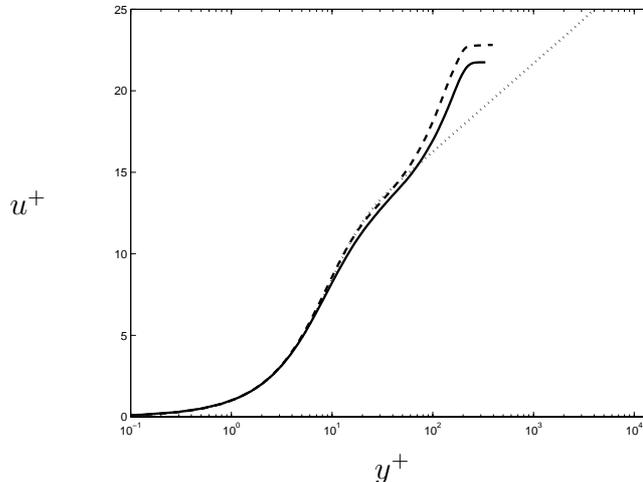
FIGURE 5.1. Velocity profiles from A2 in inner scaling.
— DNS; - - DRSM; $\cdots$ Asymptotic DRSM.

There exists a number of methods to develop better models than the mixing length for ν_T. In e.g. the two-equation models ν_T is written in the form,

$$\nu_T = C_\mu \frac{K^2}{\varepsilon} \qquad \text{or} \qquad \nu_T = \frac{K}{\omega}, \tag{5.4}$$

and two transport equations for K and ε or ω have to be solved.

There are also many models not based on the Boussinesq hypothesis. In the differential Reynolds stress model (DRSM) the transport equations for the Reynolds stresses themselves are solved. This leads to a much greater computational effort than for the two-equation models. In addition, numerical issues become important. However, in some cases the DRSM is required to capture features of the flow that cannot be predicted by other models.

In the explicit algebraic Reynolds stress model (EARSM), the advection and viscous diffusion of the anisotropy are neglected in the transport equations, and an algebraic equation for the anisotropy is obtained. This kind of model is based on a two-equation model and can be written in a similar form as a generalized Boussinesq hypothesis.

In paper1 the DRSM of Hanjalić *et al.* (1995) was used to investigate the asymptotic behavior of the boundary layer for large Reynolds numbers. Furthermore, the model was used to predict the mean flow at the same low Reynolds number as the DNS. The model predictions showed that low Reynolds number effects are well captured by the DRSM. An example from the case A2 is shown in figure 5.1. The velocity profile from the low Reynolds number DNS (solid line) is well predicted by the DRSM (dashed line). The asymptotic profile calculated with the DRSM at high Reynolds number develops into a self-similar profile (dotted line).
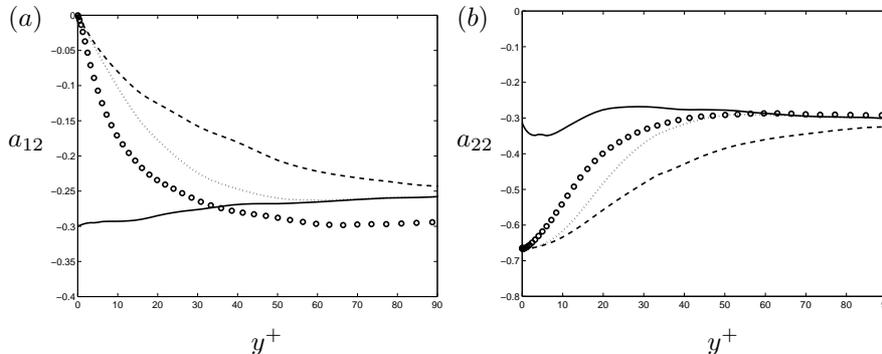
FIGURE 5.2. A3 at $x = 150$: ○ DNS; — non-damped EARSM; Damped EARSM with the scaled coordinate in f_1 as - - y^+; · · · y^*. a) a_{12}. b) a_{22}.

In paper 2 a number of two-equations models were compared with DNS data and experimental data. The general conclusion from that investigation is that the $k - \omega$ model is reasonably accurate, while the $k - \epsilon$ model gives rather large deviations for strong adverse pressure gradients.

5.1.2. *Improvement of wall damping*

In paper 5 the EARSM model of Wallin & Johansson (2000) was used for the investigation of the near-wall behavior. By using DNS data in the model expressions for the Reynolds stresses close to the wall, the influence of the wall-damping functions can be examined. The wall-damping is based on the van Driest function, equation (5.2). However, in an APG boundary layer, equation (5.2) is not valid. Some of the work in the earlier mixing length models have been concentrated on finding a relation between the constant A^+ and the pressure gradient, see e.g. Granville (1989). A different method to improve the wall-damping is used in paper 5. The viscous scaling of y in equation (5.2) is replaced with the scalings related to the work in paper 4. The improved near-wall damping is illustrated in figure 5.2, where the expressions for the anisotropy are evaluated from DNS data. The DNS data is represented with circles and the non-damped (i.e. $f_1 = 1$) model evaluation is shown as the solid line. By damping with $f_1 = 1$ based on y^+ the dashed line is obtained. If y^+ is replaced with $y^* \equiv yu_*/\nu$, where u_* is defined from equation (3.22), the dotted profile is obtained. Thus, the wall-damping is much improved by changing from the viscous scaling to the relevant scaling in an APG flow.

DNS data from the case A3 was also used by Wallin & Johansson (2000) to evaluate the damping of the EARSM model.

5.2. Instantaneous flow structures

Turbulence does not consist of randomly fluctuating velocities. The experiments of Kline *et al.* (1967) showed that low-speed streaks populate the near-wall region. Since then many different types of structures and models for the dynamics of turbulence structures have been proposed, see the introduction of paper 7.

Most models trying to capture the essential mechanisms in turbulence are conceptual, not predictive, in the sense they do not relate Reynolds stresses to the mean flow, but try to explain the various steps in the production and regeneration of turbulence. For a general review of the subject, see Robinson (1991).

In paper 7 the instability mechanism of a turbulent low-speed streak is addressed. Simulations of an artificial streak in a laminar boundary layer were performed in order to examine the instability in a controlled environment. This laminar simulation was also used for reproducing and further investigate the results from an experimental investigation by Acarlar & Smith (1987).

The laminar streak breaks down due to an instability originating from an inflectional velocity profile. The instability calculations using the Orr-Sommerfeld equations gave qualitative agreement in the growth rate and streamwise wavenumber with the corresponding values extracted from the DNS velocity fields. The instability waves riding on the streak, roll up to form a horseshoe vortex. Some striking similarities between the vortices that appear in the laminar simulation and the ones found in a ZPG turbulent boundary layer were found. To illustrate the qualitative agreement, a small part of the turbulent boundary layer is shown in figure 5.3, while the laminar streak is shown in figure 5.4. The horseshoe vortices are visualized with regions of low pressure. The light grey structures represent the low-speed streaks and the darker ones represent regions with low pressure. The flow is directed upward in the figures.
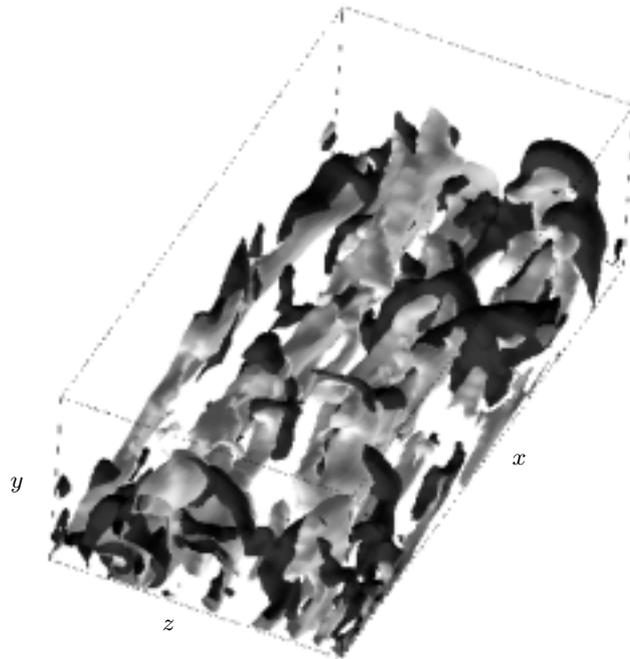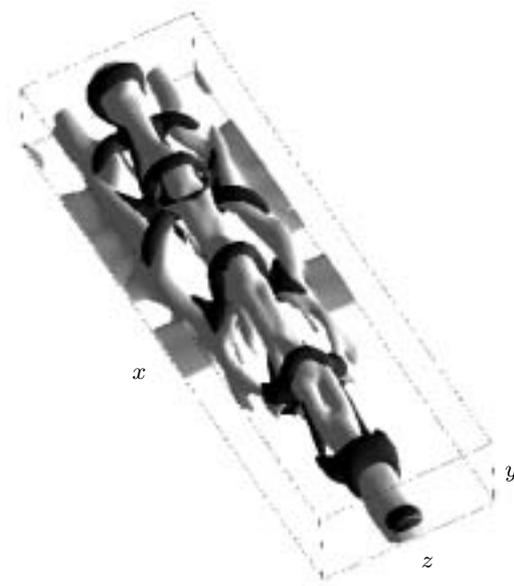
FIGURE 5.3. The turbulent boundary layer.

FIGURE 5.4. The laminar low-speed streak.

CHAPTER 6

Conclusions and outlook

The direct numerical simulations have been completed with a code which runs efficiently on all types of super computers in use today. Besides the obvious wishes for higher Reynolds number, larger computational box and higher resolution, there is a number of possible extensions for future DNS. A natural extension to this work is the turbulent boundary layer with a three-dimensional mean flow. Although some theoretical work has been presented for this type of flow, (e.g. Degani *et al.* 1993), DNS would be interesting for comparison. Wall roughness and wall curvature are also complications that are of engineering significance.

A consistent analysis of the turbulent boundary layer equations for the inner part in this work has given the theoretical expressions for the streamwise velocity profile in the viscous sub-layer and overlap region. The analysis could perhaps be extended to include complications of the kind mentioned above, see e.g. Townsend (1976).

The work on turbulence modelling leaves some unanswered questions. The damping of the non-linear terms in the EARSM model is one such issue. However, the near-wall laws for APG boundary layers developed here could be of great importance in turbulence model predictions of such flows. The laws are suitable as boundary conditions through wall functions if well defined freestream data are available. The work on coherent structures and their dynamics can be developed to obtain a more complete picture. Specially the instability mechanism of the low-speed streaks in a turbulent flow needs to be more thoroughly investigated. The concept of two instability mechanisms present in turbulence could lead to a more unified view on the self-sustained turbulence regeneration cycle. The knowledge about turbulence structures should be utilized in a predictive model, maybe in a similar manner as in the investigation of Perry *et al.* (1994).

For more specific conclusions, the reader is referred to papers 1 through 8.

Acknowledgments

First of all I wish to thank my advisor, Professor Dan Henningson, whose enthusiasm and energy never ceased to inspire me. His ability to always ask me the questions I needed for my thoughts to turn the right direction, astonished me every time.

Professor Ruud Henkes introduced me to turbulence modelling, and his numerical code was of great importance for my work. Our collaboration at TU Delft was the most productive month of my time as a Ph.d. student.

The many fruitful discussions with Professor Joseph Haritonidis during my stay at Ohio State University (OSU) in Columbus gave me insight in perhaps the most confusing part of turbulence research; coherent structures. I also wish to thank him for letting me stay in his cozy house, and introducing me to the finest cuisine of Ohio.

My stay at the Center for Turbulence Research (CTR) at Stanford University was a great opportunity to meet some of the most prominent researchers in turbulence. Professor Parviz Moin is acknowledged for letting me spend a month analyzing their DNS data base.

The financial support for my visits to OSU and CTR was partly covered with the aid of Knut och Alice Wallenbergs stiftelse and The Foundation BLANCEFLOR Boncompagni-Ludovisi, née Bildt.

The National Aerospace Laboratory (NAL) in Tokyo is acknowledged for letting me work there as an STA-fellow. This work was fully financed by the Japan Science and Technology Corporation (JST). Doctor Naoki Hirose was of invaluable help, both for work and for my life in Tokyo. I thank him also for letting me stay in his guest house in Tokyo. I also wish to thank Doctor Yuichi Matsuo for his help during my struggle with the Numerical Wind Tunnel. I will not forget those long debugging nights. My second visit to NAL was financed by The Scandinavia-Japan Sasakawa Foundation.

My colleagues at the department have provided a stimulating atmosphere. I thank you all for that and for the many interesting discussions about almost everything (and many times about nothing at all). Special thanks are sent to Doctor Krister Alvelius, whose brilliant ideas were of great help while working with the code. I also wish to thank Doctor Stefan Wallin who I had the pleasure to work with under a few but very productive brainstorming meetings.

Bibliography

ACARLAR, M. S. & SMITH, C. R. 1987 A study of hairpin vortices in a laminar boundary layer. Part 2. Hairpin vortices generated by fluid injection. *J. Fluid Mech.* **175**, 43–48.

AFZAL, N. 1996 Wake layer in a turbulent boundary layer with pressure gradient: a new approach. In *IUTAM Symposium on Asymptotic Methods for Turbulent Shear flows at High Reynolds Numbers* (ed. K. Gersten), pp. 95–118. Kluwer Academic Publishers.

BARENBLATT, G. I. 1996 *Scaling, Self-Similarity, and Intermediate Asymptotics*. Cambridge University Press.

BERTOLOTTI, F. P., HERBERT, T. & SPALART, P. R. 1992 Linear and nonlinear stability of the Blasius boundary layer. *J. Fluid Mech.* **242**, 441–474.

BOUSSINESQ, T. V. 1877 Essai sur la théorie des eaux courantes. *Mém. prés. Acad. Sci.* 3rd edn, Paris XXIII, p.46.

BRADSHAW, P. 1967 The turbulent structure of equilibrium boundary layers. *J. Fluid Mech.* **29**, 625–645.

BRADSHAW, P. & HUANG, G. P. 1995 The law of the wall in turbulent flow. *Proc. Roy. Soc. Lond. Ser. A* **451**, 165–188.

COOLEY, J. W. & TUKEY, J. W. 1965 An algorithm for the machine calculation of complex Fourier series. *Math. Comput.* **19**, 297–301.

DEGANI, A. T., SMITH, F. T. & WALKER, J. D. A. 1993 The structure of a three-dimensional turbulent boundary layer. *J. Fluid Mech.* **250**, 43–68.

VAN DRIEST, E. R. 1956 On turbulent flow near a wall. *J. Aero. Sci.* **23**, 1007–1011.

ELSBERRY, K., LOEFFLER, J., ZHOU, M. D. & WYGNANSKI, I. 2000 An experimental study of a boundary layer that is maintained on the verge of separation. *J. Fluid Mech.* **423**, 227–261.

FOURIER, J. 1822 *Théorie analytique de la chaleur*. Firmin Didot, Paris.

GRANVILLE, P. S. 1989 A modified van driest formula for the mixing length of turbulent boundary layers in pressure gradients. *J. Fluids Eng.* **111**, 94–97.

HANJALIĆ, K., JAKIRLIĆ, S. & HADŽIĆ, I. 1995 Computation of oscillating turbulent flows at transitional *Re*-numbers. In *Turbulent Shear Flows 9* (eds. F. Durst, N. Kasagi & B. E. Launder), pp. 323–342. Springer-Verlag.

HENKES, R. A. W. M. 1998 Scaling of equilibrium boundary layers under adverse pressure gradient using turbulence models. *AIAA J.* **36**, 320–326.

KIM, J., MOIN, P. & MOSER, R. 1987 Turbulence statistics in fully developed channel flow. *J. Fluid Mech.* **177**, 133–166.

KLINE, S. J., REYNOLDS, W. C., SCHRAUB, F. A. & RUNSTADLER, P. W. 1967 The structure of turbulent boundary layers. *J. Fluid Mech.* **30**, 741.

KREISS, H.-O. & OLIGER, J. 1972 Comparison of accurate methods for the integration of hyperbolic equations. *Tellus* **XXIV**, 199–215.

MELLOR, G. L. 1966 The effects of pressure gradients on turbulent flow near a smooth wall. *J. Fluid Mech.* **24**, 255–274.

MELLOR, G. L. & GIBSON, D. M. 1966 Equilibrium turbulent boundary layers. *J. Fluid Mech.* **24**, 225–253.

NA, Y. & MOIN, P. 1998 Direct numerical simulation of a separated turbulent boundary layer. *J. Fluid Mech.* **374**, 379–405.

NORDSTRÖM, J., NORDIN, N. & HENNINGSON, D. S. 1999 The fringe region technique and the fourier method used in the direct numerical simulation of spatially evolving viscous flows. *SIAM J. Sci. Comp.* **20** (4), 1365–1393.

ORSZAG, S. A. 1972 Comparison of pseudospectral ans spectral approximations. *Stud. Appl. Math.* **51**, 253–259.

ÖSTERLUND, J. M., JOHANSSON, A. V., NAGIB, H. M. & HITES, M. H. 2000 A note on the overlap region in turbulent boundary layers. *Phys. Fluids* **12**, 1–4.

PATEL, V. C. 1973 A unified view of the law of the wall using mixing-length theory. *Aeronaut. Q.* **24**, 55–70.

PERRY, A. E., MARUŠIĆ, I. & LI, J. D. 1994 Wall turbulence closure based on classical similarity laws and the attached eddy hypothesis. *Phys. Fluids* **6** (2), 1024–1035.

PRANDTL, L. 1925 Bericht über Untersuchungen zur ausgebildeten Turbulenz. *Zeitschrift für Angewandte Mathematik und Mechanik* **5**, 136.

PRANDTL, L. 1932 Zur turbulenten Strömung in Rohren und längs Platten. *Ergebn. Aerodyn. Versuchsanst. Göttingen* **4**, 18–29.

ROBINSON, S. K. 1991 Coherent motions in the turbulent boundary layer. *Ann. Rev. Fluid Mech.* **23**, 601–639.

SIMPSON, R. L. 1970 Characteristics of turbulent boundary layers at low Reynolds numbers with and without transpiration. *J. Fluid Mech.* **42**, 769–802.

SKÅRE, P. E. & KROGSTAD, P.-Å. 1994 A turbulent equilibrium boundary layer near separation. *J. Fluid Mech.* **272**, 319–348.

SKOTE, M. & HENNINGSON, D. 1997 Direct numerical simulation of turbulent boundary layers with adverse pressure gradients. In *Advances in DNS/LES* (eds. C. Liu & Z. Liu), pp. 215–222. Greyden Press.

SKOTE, M. & HENNINGSON, D. 1998 Direct numerical simulation of adverse pressure gradient turbulent boundary layers. In *Advances in Turbulence VII* (ed. U. Frisch), pp. 171–174. Kluwer Academic Publishers.

SKOTE, M. & HENNINGSON, D. 1999 Dns of a turbulent boundary layers under a strong adverse pressure gradient. In *Recent Advances in DNS and LES* (eds. D. Knight & L. Sakell), pp. 373–384. Kluwer Academic Publishers.

SKOTE, M., HENNINGSON, D., HIROSE, N., MATSUO, Y. & NAKAMURA, T. 2000 Parallel dns of a separating turbulent boundary layer. In *Proceedings of Parallel CFD 2000, Trondheim.*

SPALART, P. R. 1988 Direct simulation of a turbulent boundary layer up to $Re_\theta = 1410$. *J. Fluid Mech.* **187**, 61–98.

SPALART, P. R. & COLEMAN, G. N. 1997 Numerical study of a separation bubble with heat transfer. *European J. Mechanics B/Fluids* **16**, 169.

SPALART, P. R. & LEONARD, A. 1987 Direct numerical simulation of equilibrium turbulent boundary layers. In *Turbulent Shear Flows 5* (eds. F. Durst, B. E. Launder, J. L. Lumley, F. W. Schmitd & J. H. Whitelaw), pp. 234–252. Springer-Verlag.

SPALART, P. R. & WATMUFF, J. H. 1993 Experimental and numerical study of a turbulent boundary layer with pressure gradients. *J. Fluid Mech.* **249**, 337–371.

STRATFORD, B. S. 1959a An experimental flow with zero skin friction throughout its region of pressure rise. *J. Fluid Mech.* **5**, 17–35.

STRATFORD, B. S. 1959b The prediction of separation of the turbulent boundary layer. *J. Fluid Mech.* **5**, 1–16.

TENNEKES, H. & LUMLEY, J. L. 1972 *A First Course in Turbulence*. The MIT Press.

TOWNSEND, A. A. 1956 *The structure of turbulent shear flow*. Cambridge University Press.

TOWNSEND, A. A. 1961 Equilibrium layers and wall turbulence. *J. Fluid Mech.* **11**, 97–120.

TOWNSEND, A. A. 1976 *The Structure of Turbulent Shear Flow*. Cambridge University Press.

WALLIN, S. & JOHANSSON, A. V. 2000 An explicit algebraic Reynolds stress model for incompressible and compressible turbulent flows. *J. Fluid Mech.* **403**, 89–132.

WILCOX, D. C. 1993 *Turbulence Modeling for CFD*. DCW Industries, Inc.